Optical measurement of cell membrane tension

Gabriel Popescu[1], Takahiro Ikeda[2], Keisuke Goda[3], Catherine A. Best-Popescu[4], Michael Laposata[4], Suliana Manley[5], Ramachandra R. Dasari[1], Kamran Badizadegan[1], and Michael S. Feld[1]

[1]) George R. Harrison Spectroscopy Laboratory Massachusetts Institute of Technology, Cambridge, MA 02139

[2]) Hamamatsu Photonics K.K., 5000 Hirakuchi, Hamamatsu, Shizuoka 434-8601 Japan

[3]) Department of Physics, Massachusetts Institute of Technology, Cambridge, MA 02139

[4]) Department of Pathology, Massachusetts General Hospital and Harvard Medical School, Boston, MA 02114

[5]) Department of Chemical Engineering, Massachusetts Institute of Technology, Cambridge, MA 02139

Phys. Rev. Lett.

In press

Abstract

Using a novel non-contact technique based on optical interferometry, we quantify the nanoscale thermal fluctuations of red blood cells (RBCs) and giant unilamellar vesicles (GUVs). The measurements reveal a non-vanishing tension coefficient for RBCs, which increases as cells transition from a discocytic shape to a spherical shape. The tension coefficient measured for GUVs is, however, a factor of 4-24 smaller. By contrast, the bending moduli for cells and vesicles have similar values. This is consistent with the cytoskeleton confinement model, in which the cytoskeleton inhibits membrane fluctuations (Gov et al., Phys. Rev. Lett., 90, 228101, 2003).

PACS numbers: 87.68.+z, 87.15.Ya.

The red blood cell (RBC) has a composite membrane consisting of a lipid bilayer coupled to a two-dimensional spectrin network, which confers to the cell its characteristic properties of simultaneous softness and strong shear elasticity[1, 2]. Because RBCs have a relatively simple structure, they represent a convenient model for studying cell membranes, which have broad applications in both science and technology[3, 4]. The lipid bilayer is 4-5 nm thick, and exhibits fluidlike behavior, characterized by a finite bending modulus κ and a vanishing shear modulus, $\mu \approx 0$. The resistance to shear, crucial for RBC function, is provided by the spectrin network, which has a mesh size of ~80 nm.

Spontaneous membrane fluctuations, or "flickering", have been modeled theoretically under both static and dynamic conditions in an attempt to connect the statistical properties of the membrane displacements to relevant mechanical properties of the cell[5-9]. These thermally-induced membrane motions exhibit 100 nm scale amplitudes at frequencies of tens of Hz. In past studies, measurements of the membrane mean squared displacement vs. spatial wave vector, $\Delta u^2(q)$, revealed a q^{-4} dependence predicted by the equipartition theorem, which is indicative of fluidlike behavior[6, 10-13]. These results conflict with the static deformation measurements provided by micropipette aspiration[14, 15], high-frequency electric fields[16, 17], and, more recently, optical tweezers[18], which indicate an average value for the shear elasticity of the order of $\mu \sim 10^{-6} J/m^2$. Gov et al. predicted that the cytoskeleton pinning of the membrane has an overall effect of confining the fluctuations and, thus, gives rise to superficial tension much larger than in the case of free bilayers[5]. This confinement model may offer new insight into the cytoskeleton-bilayer interaction that determines the morphology and physiology of the cell[19].

RBCs lack nuclei and organelles and can be assumed optically homogeneous, i.e. characterized by a constant refractive index. Therefore, measurement of the cell optical path-length via interferometric techniques can provide information about the physical topography of the membrane with sub-wavelength accuracy and without contact. However, existing optical methods, including phase contrast microscopy (PCM)[6], reflection interference contrast microscopy (RICM)[10], and fluorescence interference contrast (FLIC)[20] are limited in their ability to measure cell membrane displacements. It is well known that PCM provides phase shifts quantitatively only for samples that are optically much thinner than the wavelength of light, which is a condition hardly satisfied by any cell type. Similarly, a single RICM measurement cannot provide the absolute cell thickness unless additional measurements or approximations are made[21]. FLIC relies on inferring the absolute position of fluorescent dye molecules attached to the membrane from the absolute fluorescence intensity, which may limit both the sensitivity and acquisition rate of the technique[20]. Thus, none of these techniques is suitable for making spatially-resolved measurements of the dynamics of cell membrane fluctuations, and testing the hypothesis of Gov et al.

In this Letter, we present highly sensitive experimental measurements of thermal fluctuations associated with GUVs and RBCs under different morphological conditions. The results reveal the effect of the cytoskeleton on the RBC fluctuations and support the model proposed by Gov et al. In order to quantify membrane fluctuations at the nanometer and millisecond scales with high transverse resolution, we developed a new quantitative phase imaging technique. The method combines Hilbert phase microscopy (HPM)[22, 23] developed in our laboratory with an electronic stabilization feedback loop and

is referred to as the stabilized Hilbert phase microscopy (sHPM). The principle of the measurement extends the concept of complex analytic signals to the spatial domain by interfering the high-resolution microscope image field with a reference plane wave. The experimental geometry is depicted in Fig. 1. The 632.8 nm radiation from a HeNe laser is collimated and divided into a sample (S) and reference (R) arm to form a modified Mach-Zender interferometer. The sample beam provides the illumination field for an inverted microscope equipped with an immersion 100X (NA=1.2) objective that allows for a transverse resolution of 0.26 μm. The tube lens is positioned such that the image of the sample is formed at the CCD plane via the beam splitter cube BS. The reference field is collimated and expanded by a telescopic system consisting of another microscope objective and the same tube lens. At the CCD plane, this reference beam can be approximated by a plane wave, which interferes with the image field. The reference field is tilted with respect to the sample field such that uniform fringes are created at an angle of 45^{o} with respect to the x and y axes. The CCD used (C7770, Hamamatsu Photonics) has an acquisition rate of 291 frames/ s at 640x480 pixels per image the fringes are sampled by 4-6 CCD pixels per period. Using high-pass spatial filtering and Hilbert transformation, the spatially varying phase $\phi(x, y)$ associated with the microscope image is retrieved in each point from a single-exposure image[22]. However, this geometry is susceptible to inherent optical path-length noise, which prevents accurate measurements of RBC dynamics. In order to suppress this noise, we used a stabilization feedback system that locks the interferometer on an interference fringe. The feedback circuit actively operates via a piezo-electric transducer (PZT) in the reference arm, using a combination of spatial and temporal modulation, as follows. A small mirror M deflects a

portion of the interfering beams before they reach the CCD. At a plane conjugate to the image (CCD) plane, we place an amplitude grating, which has the same period as the interferogram. Due to this spatial matching, each diffraction order *n* produced by the sample beam overlaps with the order *n-1* of the reference beam. The two interfering beams propagating on axis are spatially isolated by an aperture and detected by the photodiode PD. The feedback loop operates on a principle similar to that described in Ref.[24]. The PD signal is mixed with the local oscillator (LO) that modulates the reference arm length, and then is low-pass filtered, yielding the error signal. The frequency of the LO is chosen to be $\Omega/(2\pi)$ = 15kHz such that the displacements of the sample can be measured up to about 1kHz. The control signal that corrects the reference arm length with respect to the sample arm against the fringe fluctuations is combined with the LO modulation signal and fed to the PZT. The stability of the instrument against the residual noise was assessed by acquiring successive phase images of the field of view with no sample. The optical path-length standard deviation σ_s calculated from 128 phase images at 10 ms/ frame was calculated for each pixel. The inset of Fig. 1 shows the histogram of the standard deviation obtained from an area of 100x100 pixels. The average standard deviation had a value of 1.2 nm, which demonstrates the efficacy of the active stabilization and suitability of the instrument for quantifying membrane motions. This combination of HPM and active stabilization allows for accurate quantitative measurements of cell membrane fluctuations and represents a significant improvement with respect to our previous reports[22, 23].

In order to investigate the physical difference between RBC membrane and free bilayer fluctuations, we measured the fluctuations of giant unilamellar vesicles. The

membrane composition we used was 100% SOPC (1-Stearoyl-2-Oleoyl-sn-Glycero-3-Phosphocholine). The unilamellar vesicles were electroformed for 2 hours under a 1 V, 10 Hz AC field in a 300 mM glucose solution[25] and diluted in a sucrose solution for increased optical contrast, and to slightly deflate the vesicles. The refractive index contrast with respect to the surrounding fluid, $\Delta n = 0.011$, was obtained from the quantitative phase image by assuming a spherical profile for the vesicles. Sets of 1,000 time-resolved phase images of individual GUVs were recorded at 10.3 ms/ frame. The vesicles under investigation ranged in diameter from 8-12 μm and their thickness profile was obtained from phase images as $u(x,y;t) = (\lambda / 2\pi\Delta n)\phi(x,y;t)$. Each 1,000 frame data set was then separated into groups of 128 frames, analyzed separately to obtain mean squared displacements, and finally averaged to provide statistically significant information for each vesicle. Using Fourier transformations both in time and space, we obtained the mean squared displacement as a function of spatial wave vector and temporal frequency, $\Delta u^2(\boldsymbol{q},\omega)$. Figure 2 summarizes the static (spatial) behavior of the thermal fluctuations averaged over 5 vesicles, $\Delta u^2(q) = \int \Delta u^2(q,\omega) d\omega$, with $q = |\boldsymbol{q}|$. The data can be fitted very well over the spatial wave vector interval $1 < q < 13$ rad/μm by the equation[6]

$$\Delta u^2(q) = \frac{k_B T}{\kappa q^4 + \sigma q^2}, \qquad (1)$$

where k_B is the Boltzmann constant and T=298 K is the absolute temperature for our experiments. The measured values at low-q deviate from this form; however, this is expected for wavelengths corresponding to the size of the vesicles. The only two parameters used for the fit are the tension coefficient, σ, and the bending modulus, κ. The

value for the bending modulus obtained from the fit is $\kappa = (0.7 \pm 0.12) \times 10^{-20} J$ and the tension coefficient was $\sigma = (3.5 \pm 0.6) \times 10^{-7}$ J/m^2. These values agree very well with what was measured on vesicles using pipette aspiration [26].

Blood samples were collected and centrifuged for 10 minutes at an acceleration of 2000 g and temperature of 5^{o}C to separate RBCs from plasma. The cells were washed three times with saline solution and finally suspended in phosphate buffered saline (pH 7.4), as described in Ref.[27]. The RBCs were then placed between cover slips and imaged without additional preparation. Using a refractive index contrast $\Delta n = 6\%$ between the hemoglobin solution contained in the cell and the surrounding fluid[28], the RBC thickness profile was directly obtained from the phase image. The membrane displacements were statistically analyzed both spatially and temporally.

Our samples were primarily composed of RBCs with a typical discocytic shape, but also contained cells with abnormal morphology which formed spontaneously in the suspension, such as echinocytes, with a spiculated shape, and spherocytes, approaching a spherical shape. By taking into account the free energy contributions of both the bilayer and cytoskeleton, these morphological changes have been successfully modeled[19]. Figures 3a-c show typical sHPM images of cells in these three groups. For comparison, we also analyzed the motions of RBCs fixed with 40μM gluteraldehyde using a standard procedure[27]. The resultant mean squared displacements, $\Delta u^2(q)$, for each group of 4-5 cells are summarized in Fig. 3d. The fixed cells show significantly diminished fluctuations, as expected. The curves associated with the three untreated RBC groups exhibit a power law behavior with an exponent $\alpha = 2$. As in the case of vesicles, this dependence is an indication of tension; however, the RBC tension is determined by the

confinement of the bilayer by the cytoskeleton[5, 29]. Based on this model, we fitted the data to extract the tension coefficient for each individual cell. The average values obtained for the discocytes, echinocytes, and spherocytes are, respectively, $\sigma = (1.5 \pm 0.2) \cdot 10^{-6}\ J/m^2$, $\sigma = (4.05 \pm 1.1) \cdot 10^{-6}\ J/m^2$, and $\sigma = (8.25 \pm 1.6) \cdot 10^{-6}\ J/m^2$. Thus our data indicates the existence of positive tension in the membrane, which agree very well with the simulation by Discher et al. [30]. The tension coefficient of red blood cells is 4-24 times larger than that of vesicles, which suggests that the contribution of the cytoskeleton might be responsible for this enhancement. Further, it is known that the cytoskeleton plays a role in the transitions from a normal red blood cell shape to abnormal morphology, such as echinocyte and spherocyte[19]. Therefore the consistent increase in tension we measured for the discocyte-echinocyte-spherocyte transition can be explained by changes in the cytoskeleton, which pins the bilayer. These findings support the hypothesis that the fluctuations are laterally confined by a characteristic length, $\xi_0 = 2\pi\sqrt{\kappa/\sigma}$, which is much smaller than the cell size[5]. We propose that this characteristic length scale is directly measurable as a transverse coherence length of the membrane motions. In this picture, by pinning the bilayer, the cytoskeleton defines a certain coherence area of the fluctuations, which is inversely proportional to tension. In order to calculate the coherence area of cell membranes, we applied definitions from the coherence theory of optical fields in the space-frequency domain[31]. Thus, the cross-spectral density, $\Delta u^2(\rho, \omega)$, is a measure of the spatial correlations between two points separated by a distance ρ at a particular frequency. The power spectrum of the fluctuations can be obtained as $P(\omega) = \Delta u^2(0, \omega)$. Figure 4a shows the power spectra associated with the

three groups of red blood cells. All curves exhibit power law behavior $\omega^{-\alpha}$ with slightly different exponent values, $1.15 < \alpha < 1.54$, which is compatible with $\alpha = 1.33$ proposed in the literature[6, 29]. Using the measured cross-spectral density, we calculated the spectral transverse coherence length as

$$\xi(\omega) = \sqrt{\frac{\int \rho^2 \Delta u^2(\rho,\omega)\rho d\rho}{\int \Delta u^2(\rho,\omega)\rho d\rho}} \qquad (2)$$

The transverse coherence length ξ_0 was obtained by averaging $\xi(\omega)$ over frequency. This information was used to extract the bending modulus of the RBCs, given by $\kappa = \sigma\left[\xi_0/(2\pi)\right]^2$. Figure 4b shows the values measured for both the tension coefficient and bending modulus vs. the root mean squared (rms) displacement, $\Delta u_{rms} = \sqrt{2\pi\int \Delta u^2(q) q dq}$. Remarkably, the bending moduli for the different red blood cell shapes have similar values, $\kappa = (0.75 \pm 0.15)\times 10^{-20}$. This result supports our hypothesis that the difference in the fluctuations can be explained by renormalizing only one parameter, the characteristic length, which defines the coherence area of the motions. In addition, the κ values obtained for all the RBC groups are in very good agreement with those for vesicles, which suggests that the slight differences in composition between the two structures do not affect significantly their bending properties.

In summary, our measurements demonstrate the existence of tension in red blood cells of various shapes and giant unilamellar vesicles. The tension coefficient measured in red blood cells has significantly larger values than in vesicles and increases as the cell transitions from a discocyte to a spherocyte. These findings demonstrate the effect of the cytoskeleton, which can be accounted for by a proper renormalization of the coherence

area of the fluctuations. Future studies in our laboratory will address the frequency dependence of the fluctuations, such as shown in Fig. 4a, which relates to membrane rheology. Compared to other optical techniques used for studying membrane fluctuations, the sHPM technique used here is quantitative in terms of membrane topography and displacements, highly sensitive to the nanoscale membrane motions, and provides high transverse resolution.

References

1 D. Boal, *Mechanics of the cell* (Cambridge University Press, 2002).
2 R. M. Hochmuth and R. E. Waugh, Ann. Rev. Physiol. **49**, 209 (1987).
3 R. Lipowsky, Nature **349**, 475 (1991).
4 E. Sackmann, Science **271**, 43 (1996).
5 N. Gov, A. G. Zilman, and S. Safran, Phys. Rev. Lett. **90**, 228101 (2003).
6 F. Brochard and J. F. Lennon, J. Physique **36**, 1035 (1975).
7 N. Gov, Phys. Rev. Lett. **93**, 268104 (2004).
8 N. S. Gov and S. A. Safran, Biophys. J. **88**, 1859 (2005).
9 R. Lipowski and M. Girardet, Phys. Rev. Lett. **65**, 2893 (1990).
10 A. Zilker, H. Engelhardt, and E. Sackmann, J. Physique **48**, 2139 (1987).
11 K. Zeman, E. H., and E. Sackman, Eur. Biophys. J. **18**, 203 (1990).
12 A. Zilker, M. Ziegler, and E. Sackmann, Phys. Rev. A **46**, 7998 (1992).
13 H. Strey, M. Peterson, and E. Sackmann, Biophys J **69**, 478 (1995).
14 D. E. Discher, N. Mohandas, and E. A. Evans, Science **266**, 1032 (1994).
15 R. M. Hochmuth, P. R. Worthy, and E. A. Evans, Biophys J **26**, 101 (1979).
16 H. Engelhardt and E. Sackmann, Biophys J **54**, 495 (1988).
17 H. Engelhardt, H. Gaub, and E. Sackmann, Nature **307**, 378 (1984).
18 S. Suresh, J. Spatz, J. P. Mills, et al., Acta Biomaterialia **1**, 15 (2005).
19 H. W. G. Lim, M. Wortis, and R. Mukhopadhyay, Proc Natl Acad Sci U S A **99**, 16766 (2002).
20 Y. Kaizuka and J. T. Groves, Phys. Rev. Lett. **96** (2006).
21 A. Zidovska and E. Sackmann, Phys. Rev. Lett. **96** (2006).
22 T. Ikeda, G. Popescu, R. R. Dasari, et al., Opt. Lett. **30**, 1165 (2005).
23 G. Popescu, T. Ikeda, C. A. Best, et al., J. Biomed. Opt. Lett. **10**, 060503 (2005).
24 R. W. P. Drever, J. L. Hall, F. V. Kowalski, et al., Appl. Phys. B-Photophysics And Laser Chemistry **31**, 97 (1983).
25 M. I. Angelova, S. Soleau, P. Meleard, et al., Progress in Colloid and Polymer Science **89**, 122 (1992).
26 E. Evans and W. Rawicz, Phys. Rev. Lett. **64**, 2094 (1990).
27 C. A. Best, J. E. Cluette-Brown, M. Teruya, et al., J Lipid Res **44**, 612 (2003).
28 M. Hammer, D. Schweitzer, B. Michel, et al., Appl Opt **37**, 7410 (1998).
29 N. Gov, A. Zilman, and S. Safran, Biophys. J. **84**, 486A (2003).
30 D. E. Discher, D. H. Boal, and S. K. Boey, Biophys. J. **75**, 1584 (1998).
31 L. Mandel and E. Wolf, *Optical coherence and quantum optics* (Cambridge University Press, Cambridge, 1995).

FIGURE CAPTIONS

Figure 1. Stabilized Hilbert phase microscope. PZT, piezo-electric transducer; Obj, microscope objective; BS, beam splitter cube; M, mirror; PD, photodetector; G, amplifier; HP, high-pass filter; LP, low-pass filter.

Figure 2. Mean squared displacements of giant unilamellar vesicles fitted with Eq. 1, as indicated. The solid lines are guides to the eye, demonstrating the asymptotic behavior. The inset shows the phase image of a vesicle, with the colorbar in radians.

Figure 3. a-c) sHPM images of a discocyte (a), echinocyte (b), and spherocyte (c). The colorbar shows thickness in microns. d) Mean squared displacements for the three RBC groups and for the gluteraldehyde (GA) fixed cells.

Figure 4. a) Power spectrum associated with the three RBC groups, as indicated. For clarity, the curves are scaled by different factors, as shown. The solid lines represent fits with the power law functions indicated in the legend. b) Tension factor and bending modulus vs. the *rms* fluctuations for RBCs of different shapes and vesicles: s- spherocyte, e- echinocyte, d- discocyte, v- vesicle.

Fig. 1

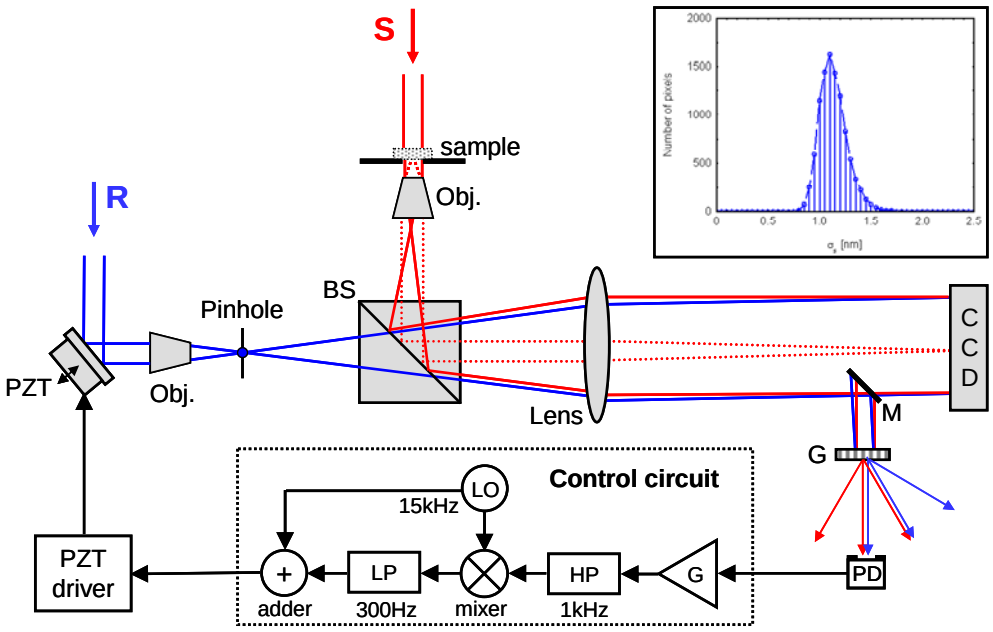
S
sample
Obj.
R
Pinhole
BS
PZT
Obj.
Lens
C
C
D
M
G
Control circuit
LO
15kHz
PZT
driver
+
adder
LP
300Hz
mixer
HP
1kHz
G
PD
number of pixels
2000
1500
1000
500
0
0
0.5
1.0
1.5
2.0
2.5

Fig. 2

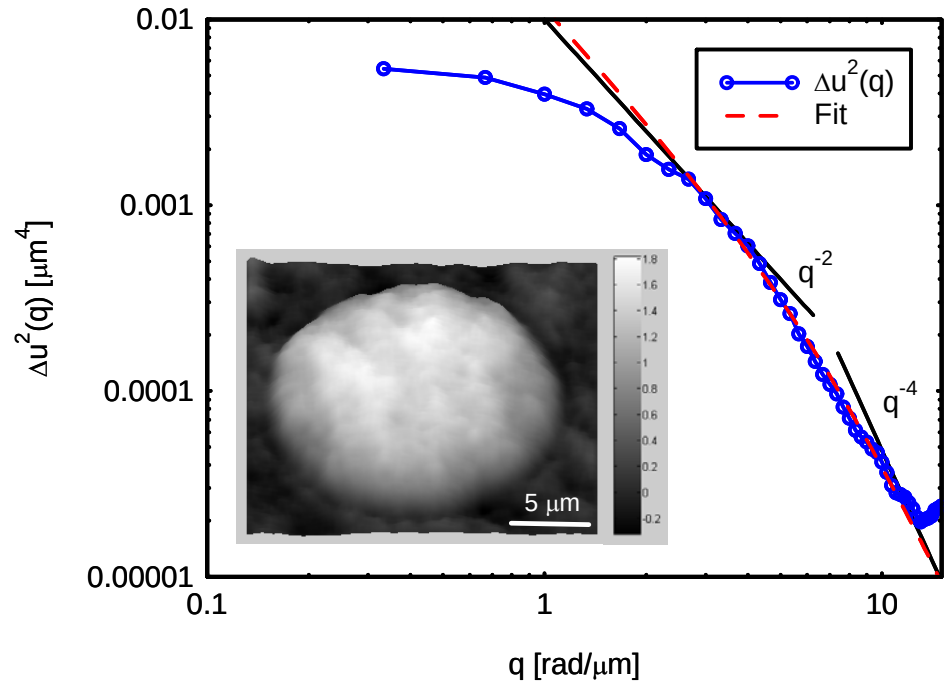
0.01
0.001
0.0001
0.00001
0.1
1
10
$\Delta u^2(q)$ [μm^4]
q [rad/μm]
$\Delta u^2(q)$
Fit
q^{-2}
q^{-4}
5 μm

Fig. 3

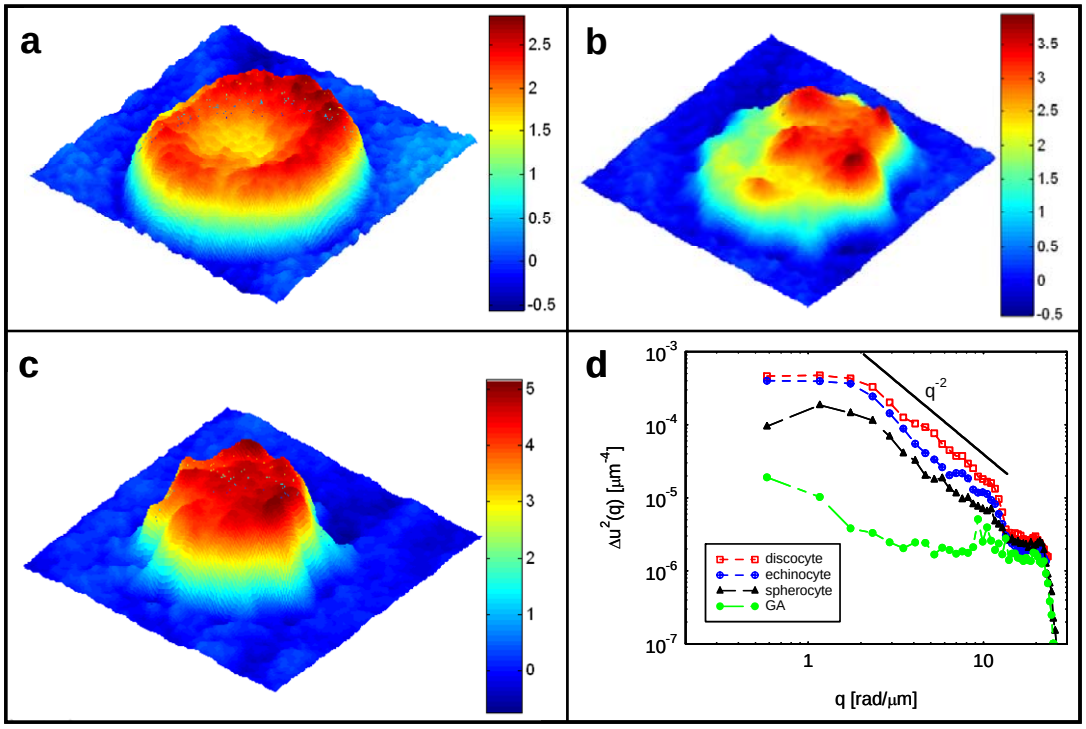
a
2.5
2
1.5
1
0.5
0
-0.5
b
3.5
3
2.5
2
1.5
1
0.5
0
-0.5
c
5
4
3
2
1
0
d
10^{-3}
10^{-4}
10^{-5}
10^{-6}
10^{-7}
$\Delta u^2(q)$ [μm^{-4}]
q^{-2}
discocyte
echinocyte
spherocyte
GA
1
10
q [rad/μm]

Fig. 4

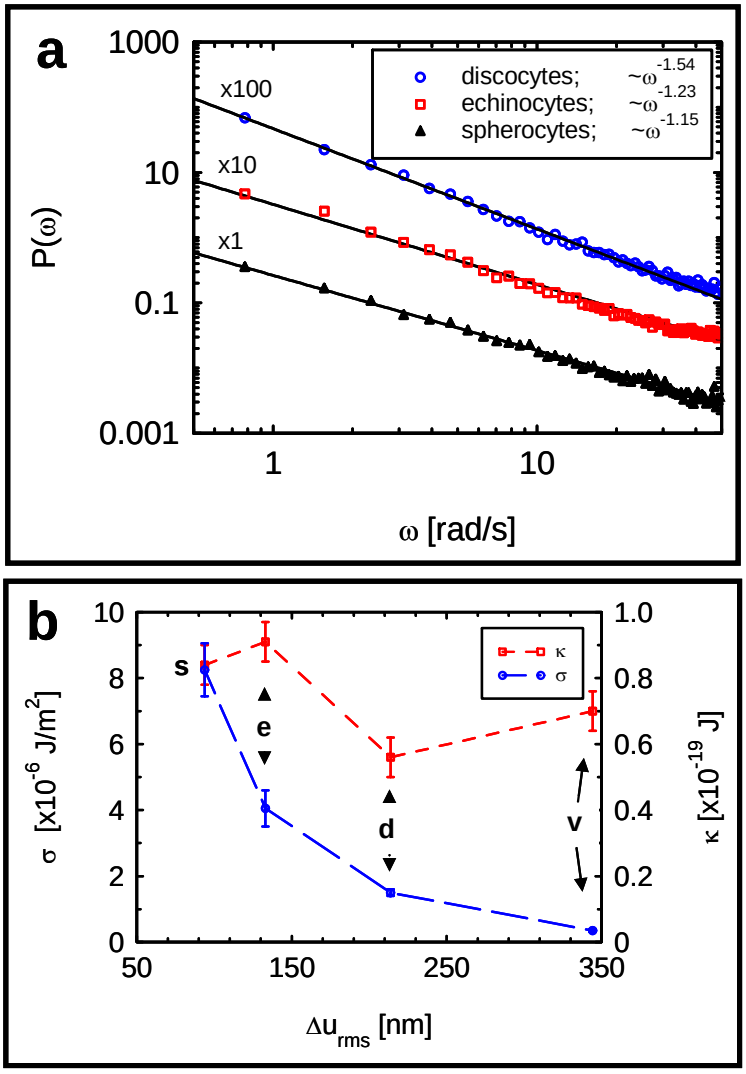
a
1000
10
0.1
0.001
P(ω)
x100
x10
x1
discocytes; ~ω^-1.54
echinocytes; ~ω^-1.23
spherocytes; ~ω^-1.15
1
10
ω [rad/s]
b
10
8
6
4
2
0
σ [x10^-6 J/m^2]
1.0
0.8
0.6
0.4
0.2
0
κ [x10^-19 J]
κ
σ
s
e
d
v
50
150
250
350
Δu_rms [nm]